J. Mater. Environ. Sci. 5 (6) (2014) 1691-1702
ISSN : 2028-2508
CODEN: JMESCN

Corrosion inhibition of α-brass in HNO_3 by indole and 2-oxyindole

A.S. Fouda*, K. Shalabi, H. Elmogazy
Chemistry Department, Faculty of Science, Mansoura University, Mansoura-35516, Egypt, email:asfouda@mans.edu.eg, Fax: +2 050 2246254 Tel: +2 050 2365730

Received 7 Dec 2013, Revised 16 July 2014, Accepted 17 July 2014
email: asfouda@hotmail.com, Fax: +20502246254, Tel: +20502365730

Abstract
The influence of indole and 2-oxyindole on the corrosion rate of α-brass in 1M HNO_3 was investigated using weight loss, potentiodynamic polarization, electrochemical impedance spectroscopy (EIS) and electrochemical frequency modulation (EFM) techniques. It was found that the investigated compounds behave as inhibitors. The inhibition efficiency increases with increasing the inhibitor concentration, but decreases with increasing the temperature. The adsorption of these compounds on the α-brass surface follows Langmuir's adsorption isotherm. The electrochemical results indicated that all the investigated compounds act as mixed-type inhibitors. Some thermodynamic parameters for corrosion processes were determined and discussed. The results obtained from chemical and electrochemical techniques were in good agreement.

*Keywords:*Corrosioninhibition; α-brass; HNO_3; Indole; oxyindole, EIS

1. Introduction
Brass has been widely used as tubing material for condensers and heat exchangers in various cooling water systems [1-7]. Brass is susceptible to a corrosion process known as dezincification and this tendency increases withincreasing zinc content of the brass [8, 9]. During the past decade, many techniques have been usedto minimize the dezincification and corrosion of brasses.Particularly, heterocyclic organic compounds containing nitrogen, sulphur and/or oxygen atoms are often used to protect metals from corrosion, e.g. aminopyrazole [10-12], amino-thiazole, triazole and thiols [13-14], phenylhydrazone derivatives [15], amino acids [16], cysteine and Glycine [17] found many applications in corrosion inhibition of copper alloys. A number of studies have recently appeared in the literature[17-22] on the topic of the corrosion inhibition of α-brass in acidic medium. But little work appears to have been done on the inhibition of α-brass alloy in HNO_3using indole derivatives.
The aim of this paper is to investigate the inhibition efficiency of indole and 2-oxyindole towards the corrosion of commercial α-brass in 1M HNO_3solutions using weight loss, potentiodynamic polarization and electrochemical impedance spectroscopy techniques.

2. Experimental
2.1 Materials
The experiments were performed with local commercial α-brass (Helwan Company of Non-Ferrous Industries, Egypt) with the following composition (weight %) Cu 67.28, Pb 0.029, Fe 0.002, Zn 32.689

2.2 Solutions
The aggressive solutions, 1M HNO_3 were prepared by dilution of analytical grade (67.5%) HNO_3 with bidistilled water.All the investigated compounds were obtained from Aldrich chemical company. All chemicals and reagents were of analytical grade. The measurements were performed in 0.5 M HCl without and with the presence of the investigated compounds in the concentration range from$1x10^{-6}$ to $1x10^{-4}$ M.The names and molecular structures of the investigated compounds are shown below.

2.3Weight lose measurements
Seven parallel α-brass sheets of 2× 2 × 0.6 cm were abraded with emery paper (grade 320–1200) and then washed with bi-distilled water and acetone. After accurate weighing, the specimens were immersed in a 100 ml beaker, which contained 100 ml of HNO_3 with and without addition of different concentrations of the investigated compounds.All the aggressive acid solutions were open to air. After 3 h, the specimens were taken out, washed, dried, and weighed accurately. The average weight loss of the seven parallel α-brass sheets could be obtained. The inhibition efficiency (IE%) and the degree of surface coverage, θ, of investigated compounds for the corrosion of α-brass in HNO_3were calculated from Eq. (1) [23]:

$$IE\ \% = \theta \times 100 = [1- (W / W°))] \times 100 \quad (1)$$

where W° and W are the values of the average weight losses without and with addition of the inhibitor, respectively.

inhibitors	Structure	Molecular weight	Chemical formula
Indole		117.15	C_8H_7N
2-Oxyindole		133.15	C_8H_7NO

2.4 Electrochemical measurements

Electrochemical experiments were performed using a typical three-compartment glass cell consisted of the α-brass specimen as working electrode (1 cm^2), saturated calomel electrode (SCE) as a reference electrode and a platinum foil (1 cm^2) as a counter electrode. The reference electrode was connected to a Luggin capillary and the tip of the Luggin capillary is made very close to the surface of the working electrode to minimize IR drop. All the measurements were done in solutions open to atmosphere under unstirred conditions. All potential values were reported versus SCE. Prior to every experiment, the electrode was abraded with successive different grades of emery paper, degreased with acetone and washed with bi-distilled water and finally dried. Tafel polarization curves were obtained by changing the electrode potential automatically from (-0.5 to 0.5 V vs. SCE) at open circuit potential with a scan rate of 1 mVs^{-1}. Stern-Geary method [24] used for the determination of corrosion current is performed by extrapolation of anodic and cathodic Tafel lines to a point which gives log i_{corr} and the corresponding corrosion potential (E_{corr}) for inhibitor free acid and for each concentration of inhibitors. Then i_{corr} was used for calculation of inhibition efficiency (IE %) and surface coverage (θ) from Eq. (2):

$$IE\ \% = \theta \times 100 = [1- (i_{corr(inh)} / i_{corr(free)})] \times 100 \quad (2)$$

where$i_{corr(free)}$ and $i_{corr(inh)}$ are the corrosion current densities in the absence and presence of inhibitor, respectively.

Impedance measurements were carried out in frequency range from 100 kHz to 0.1Hz with amplitude of 5 mV peak-to-peak using ac signals at open circuit potential. The experimental impedance was analyzed and interpreted based on the equivalent circuit. The main parameters deduced from the analysis of Nyquist diagram are the resistance of charge transfer $R_{ct}$and the capacitance of double layer C_{dl}. The inhibition efficiencies (IE %) and the surface coverage (θ) obtained from the impedance measurements are defined by Eq. (3):

$$IE\ \% = \theta \times 100 = [1- (R°_{ct} /R_{ct})]x100 \quad (3)$$

whereR^o_{ct} and R_{ct} are the charge transfer resistance in the absence and presence of inhibitor, respectively.

Electrochemical frequency modulation, EFM, was carried out using two frequencies 2 and 5 Hz. The base frequency was 0.1 Hz, so the wave form repeats after 1 s. The higher frequency must be at least two times the lower one. The higher frequency must also be sufficiently slow that the charging of the double layer does not contribute to the current response. Often, 10 Hz is a reasonable limit. The Intermodulation spectra contain current responses assigned for harmonical and intermodulation current peaks. The larger peaks were used to calculate the corrosion current density (i_{corr}), the Tafel slopes (βc and βa) and the causality factors CF2& CF3 [25, 26]. The electrode potential was allowed to stabilize for 30 min before starting the measurements. All the experiments were conducted at 25 ± 1°C. Measurements were performed using Gamry Instrument Potentiostat/ Galvanostat/ ZRA (PCI4-G750). This includes a Gamry framework system v6.03 Gamry applications include DC105 software for DC corrosion measurements, EIS300 software for electrochemical impedance spectroscopy measurements and EFM 140 for electrochemical frequency modulationmeasurements along with a computer for collecting data. Echem analyst v6.03 software was used for plotting, graphing, and fitting data.

2.5 Quantum calculation

All the quantum chemical study has been carried out using PM3 semi-empirical method, available by Spartan version 10.1. Molecular orbital calculation was based on semi-empirical method. This method has been used with full geometry optimization.

3. Results and Discussion

3.1. Chemical Method (Weight-loss measurements)

The weight loss-time curves of α-brass with the addition of indole in 1M HNO_3 at various concentrations is shown in Fig. 1. The curves of Fig. 1shows that the weight loss values of α-brass in 1M HNO_3 solutions containing the indole decrease as the concentration of the inhibitor increases; i.e., the corrosion inhibition strengthens with the inhibitor concentration, this is appear in the Table 1.

This trend may result from the fact that the adsorption of inhibitor on the α-brass increases with the inhibitor concentration, thus the α-brass surface is efficiently separated from the medium by the formation of a film on its surface [27].

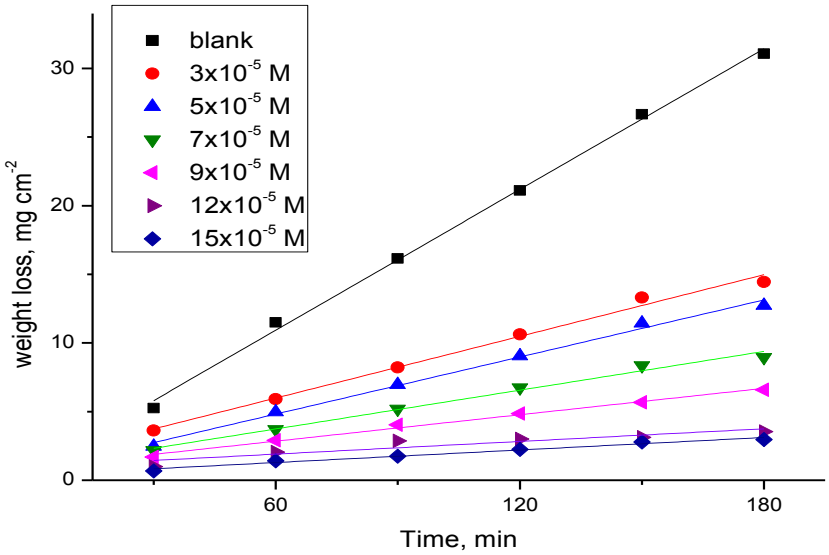

Figure 1. Weight loss- time curves for the corrosion of α-brass in 1M HNO_3in the absenceand presence of different concentrations of indole at 25°C.

Obtained values of IE% are given in Table (1), the order of decreasing inhibition efficiency of the investigated compounds is as follows:2-oxyindole> indole.

Table 1. Variation of inhibition efficiency (IE %) of investigated compounds with their molar concentrations at 25°C from weight loss measurements at 120 min immersion of α-brass in 1 M HNO_3

Conc., M	Indole		2-Oxyindole	
	θ	IE%	θ	IE%
$3x10^{-5}$	0.497	49.7	0.556	55.6
$5 x10^{-5}$	0.569	56.9	0.618	61.8
$7 x10^{-5}$	0.681	68.1	0.718	71.8
$9 x10^{-5}$	0.770	77.0	0.789	78.9
$12 x10^{-5}$	0.857	85.7	0.883	88.3
$15 x10^{-5}$	0.893	89.3	0.907	90.7

3.2 Adsorption Isotherm

It is generally assumed that the adsorption of the inhibitors on the metal surface is the essential step in the inhibition mechanism [28]. To calculate the surface coverage θ it was assumed that the inhibitor efficiency is due mainly to the blocking effect of the adsorbed species and hence IE %= 100 x θ (29). In order to gain insight into the mode of adsorption of the extract on α-brass surface, the surface coverage values from weight loss measurements were theoretically fitted into different adsorption isotherms and the values of correlation coefficient (R^2) were used to determine the best-fit isotherm. Fig. 2shows the plot C/θ vs. C which is typical of Langmuir adsorption isotherm. Perfectly linear plot was obtained with regression constant (R^2) > 0.99 and slope about unity. The Langmuir isotherm is given as [30]:

$$C/\theta = 1/K_{ads} + C \quad (4)$$

where C is the inhibitor concentration and K_{ads} is the equilibrium constant of adsorption process and is related to the standard free energy of adsorption ΔG°_{ads} by Eq. (5):

$$K_{ads}= 1/55.5 \exp (-\Delta G^{\circ}_{ads}/RT) \quad (5)$$

The value of 55.5 is the concentration of water in solution expressed in mole per liter, R is the universal gas constant and T is the absolute temperature .

The deviation of the slope from unity as observed from this study could be interpreted that there are interactions between adsorbate species on the metal surface as well as changes in adsorption heat with increasing surface coverage [31, 32], factors that were ignored in the derivation of Langmuir isotherm.

The calculated ΔG°_{ads} values were also given in Table 2. The negative values of ΔG°_{ads} ensure the spontaneity of the adsorption process and the stability of the adsorbed layer on the α-brass surface. It is well known that values of ΔG°_{ads} of the order of -40 kJ mol^{-1} or higher involve charge sharing or transfer from the inhibitor molecules to metal surface to form coordinate type of bond (chemisorption); those of order of -20 kJ mol^{-1} or lower indicate a physisorption [33, 34]. The calculated ΔG°_{ads} values (Table 2) are more negative than -20 kJ mol^{-1} indicate, therefore, that the adsorption mechanism of the investigated compounds on α-brass in 1 M HNO3 solution is typical strong physisorption and the investigated compounds are approximately constant for α-brass.

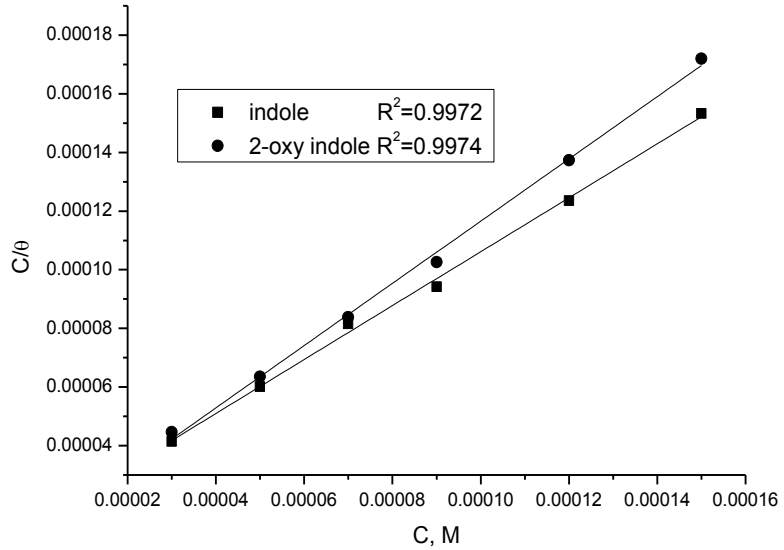

Figure 2. Curve fitting of corrosion data for α-brass in 1M HNO_3in the presence ofdifferent concentrations of indole to Langmuir adsorption isotherm at 25°C

Table 2. Equilibrium constant (K_{ads}) and adsorption free energy (ΔG°_{ads}) of investigated compounds adsorbed on α-brass surface in 1M HNO_3 at 25°C

Langmuir isotherm			
Indole		2-Oxyindole	
K_{ads}, M^{-1}	$-\Delta G^{\circ}_{ads}$, kJ $mole^{-1}$	K_{ads}, M^{-1}	$-\Delta G^{\circ}_{ads}$, kJ $mole^{-1}$
0.7059	37.6	0.9421	38.4

3.3 Effect of Temperature

The effect of temperature on the rate of corrosion of α-brass in 1MHNO_3containing different concentration of the investigated compounds was tested by weight loss measurements over a temperature range from 25 to 50°C.

The results revealed that, the rate of corrosion increases as the temperature increases and decreases as the concentration of these compounds increases for all compound used. The activation energy (E_a^*) of the corrosion process was calculated using Arrhenius equation :

$$k=A \exp(-E_a^*/RT) \quad (6)$$

where k is the rate of corrosion, A is the Arrhenius constant, R is the gas constant and T is the absolute temperature.

Figure 3 represents the Arrhenius plot in the presence and absence of $15x10^{-5}$M of investigated compounds. E_a^* values determined from the slopes of these linear plots are shown in Table 3. The linear regression (R^2) is close to 1 which indicates that the corrosion of α-brass in 1M HNO_3 solution can be elucidated using the kinetic model. Table 3 showed that the value of E_a^* for inhibited solution is higher than that for uninhibited solution, suggesting that dissolution of α-brass is slow in the presence of inhibitor and can be interpreted as due to physical adsorption [35]. It is known from Eq. 6 that the higher E_a^* values lead to the lower corrosion rate. This is due to the formation of a film on the α-brass surface serving as an energy barrier for the α-brass corrosion [36].

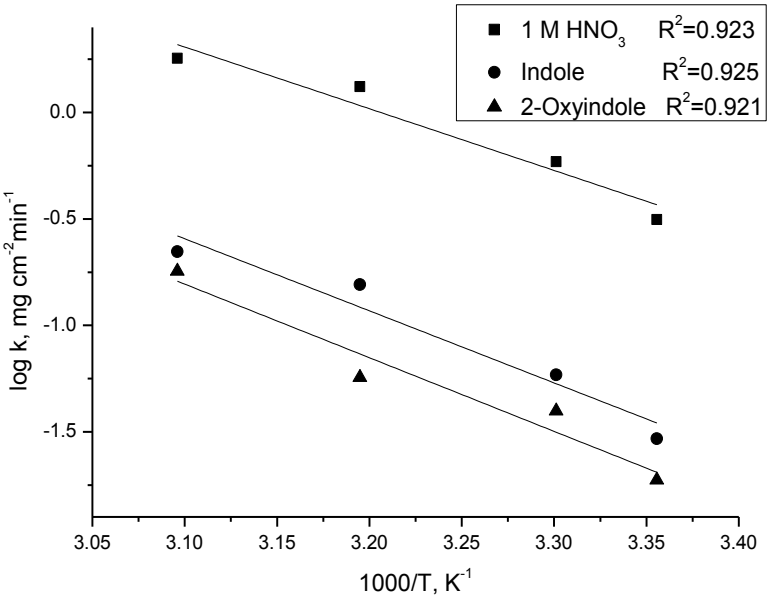

Figure 3.log k – 1/T curves for α-brass dissolution in 1 M HNO_3in the absence and presence of $5x10^{-5}$ M of indole

Enthalpy and entropy of activation (ΔH^*, ΔS^*) of the corrosion process were calculated from the transition state theory (Table 3):

$$k = (RT/ Nh) \exp (\Delta S^*/R) \exp (-\Delta H^*/RT) \quad (7)$$

where h is Planck's constant and N is Avogadro's number .A plot of log (k/ T) vs. 1/ T for α-brass in 1M HNO_3at $15x10^{-5}$M of investigated compounds, gives straight lines as shown in Fig. 4. The positive signs of ΔH^* reflect the endothermic nature of the steel dissolution process. Large and negative values of ΔS^* imply that the activated complex in the rate-determining step represents an association rather than dissociation step, meaning that decrease in disordering takes place on going from reactants to the activated complex [37, 38].

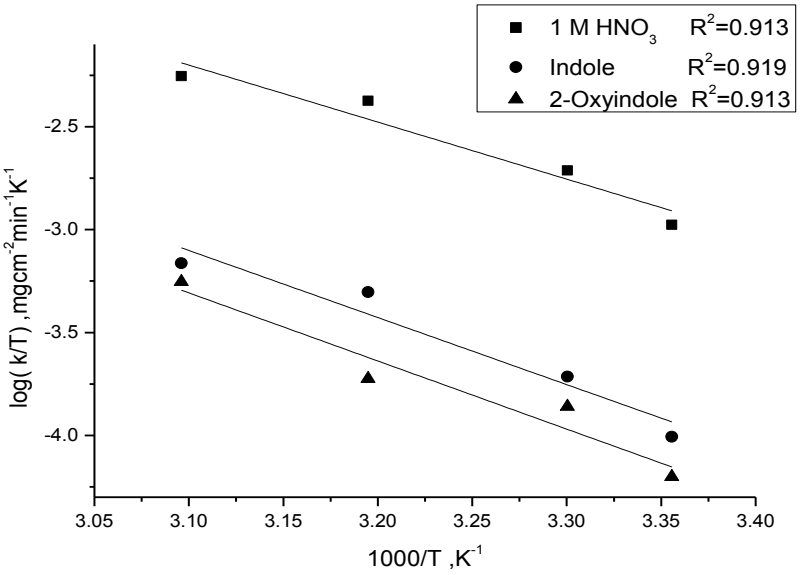

Figure 4.log k/T – 1/T curves for α-brass dissolution in 1 M HNO_3in the absence and presence of $5x10^{-5}$ M of indole

Table 3. Activation parameters of the corrosion of α-brass in 1 M HNO_3 in the absence and presence $15x10^{-5}$ M of inhibitor

Inhibitors	E_a^*, kJ mol^{-1}	ΔH^*, kJ mol^{-1}	$-\Delta S^*$, J K^{-1} mol^{-1}
1 M HNO_3	55.5	53.0	75.3
Indole	64.8	62.4	63.6
Oxyindole	66.2	63.3	64.5

3.4 PotentiodynamicPolarization Measurements

Figure 5 shows the anodic and cathodic Tafel polarization curves for α-brass in 1M HNO_3in the absence and presence of varying concentrations of indole at 25°C, respectively. From Fig. 5, it is clear that both anodic metal dissolution and cathodic H_2 reduction reactions were inhibited when investigated inhibitors were added to 1 M HNO_3 and this inhibition was more pronounced with increasing inhibitor concentration. Tafel lines are shifted to more negative and more positive potentials with respect to the blank curve by increasing the concentration of the investigated inhibitors. This behavior indicates that the undertaken additives act as mixed-type inhibitors [39,40].

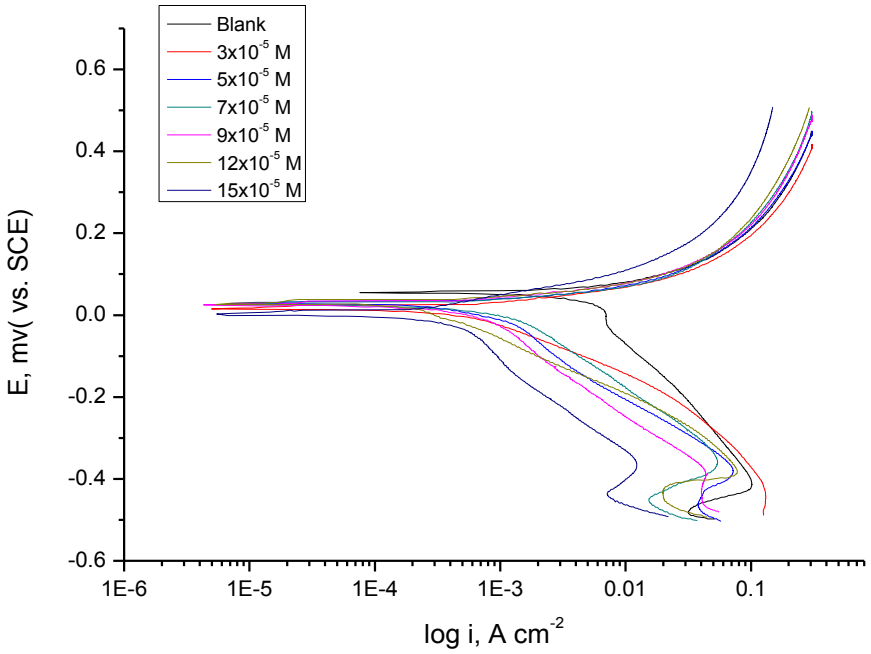

Figure 5. Potentiodynamic polarization curves for corrosion of α-brass in 1 M HNO_3in the absence and presence of different concentrations of indole at 25 ºC

The results in Table 4 show that the increase in inhibitor concentration leads to decrease the corrosion current density (i_{corr}), but the Tafel slopes (β_a , β_c),are approximately constant indicating that the retardation of the two reactions (cathodic hydrogen reduction and anodic metal dissolution) were affected without changing the dissolution mechanism [41-43].The order of decreasing inhibition efficiency of the investigated compounds is as follows: 2-oxyindole > indole

3.5 Electrochemical Impedance Spectroscopy (EIS)

The effect of inhibitor concentration on the impedance behavior of α-brass in 1M HNO_3solution at 25 ºC is presented in Fig. 6 (a,b). The curves show a similar type of Nyquist plots (Fig.6a) for α-brass in the presence of various concentrations of indole. The existence of single semi-circle showed the single charge transfer process during dissolution which is unaffected by the presence of inhibitor molecules. Deviations from perfect circular shape are often referred to the frequency dispersion of interfacial impedance, which arises due to surface roughness, impurities, dislocations, grain boundaries, adsorption of inhibitors, and formation of porous layers and in homogenates of the electrode surface [44, 45].

Inspections of the data reveal that each impedance diagram consists of a large capacitive loop with one capacitive time constant in the Bode–phase plots (Fig.6b). The electrical equivalent circuit model is shown in Fig. 7. It used to analyze the obtained impedance data. The model consists of the solution resistance (R_s), the charge-transfer resistance of the interfacial corrosion reaction (R_{ct}) and the Constant phase element (CPE).

Excellent fit with this model was obtained with our experimental data. The values of the interfacial capacitance C_{dl} can be calculated from CPE parameter values Y_0 and n using the expression [46]:

$$C_{dl} = Y_0 (\omega_{max})^{n-1} \quad (4)$$

where Y_0 is the magnitude of the CPE, ω_{max} is the angular frequency at which the imaginary component of the impedance reaches its maximum values and n is the deviation parameter of the CPE: $-1 \leq n \leq 1$.

Table 4. Effect of concentration of the investigated compounds on the free corrosion potential (E_{corr}), corrosion current density (i_{corr}), Tafel slopes (β_a & β_c), inhibition efficiency (IE%), degree of surface coverage (θ) and corrosion rate(C.R.) for the corrosion of α-brass in 1 M HNO_3 at 25°C

Inhibitor	Conc., M	i_{corr}, μA cm^{-2}	E_{corr}, mV vs SCE	β_a, $mVdec^{-1}$	β_c, $mVdec^{-1}$	C.R, mpy	Θ	IE%
1 M HNO_3		883	54	20	31	435.8	--	--
Indole	$3x10^{-5}$	452	16	133	166	223.1	0.488	48.8
	$5x10^{-5}$	448	29	60.	174	221.0	0.493	49.3
	$7x10^{-5}$	417	26	99	164	205.9	0.528	52.8
	$9x10^{-5}$	192	25	42	159	94.5	0.783	78.3
	$12x10^{-5}$	186	28	72	137	92.0	0.789	78.9
	$15x10^{-5}$	155	3	66	177	76.5	0.825	82.5
2-oxyindole	$3x10^{-5}$	358	19	55	88	176.8	0.595	59.5
	$5x10^{-5}$	120	1	52	58	59.3	0.864	86.4
	$7x10^{-5}$	91.3	6	42	71	45.0	0.897	89.7
	$9x10^{-5}$	79	-53	61	139	38.9	0.911	91.1
	$12x10^{-5}$	64.4	17	22	29	31.8	0.927	92.7
	$15x10^{-5}$	25.8	-32	48	50	12.7	0.971	97.1

EIS data (Table 5) show that the R_{ct} values increases and the C_{dl} values decreases with increasing the inhibitor concentrations. This is due to the gradual replacement of water molecules by the adsorption of the inhibitor molecules on the metal surface, decreasing the extent of dissolution reaction.
The higher (R_{ct}) values, are generally associated with slower corroding system [47, 48].The order of decreasing inhibition efficiency of the investigated compounds is as follows: 2-oxyindole > indole.

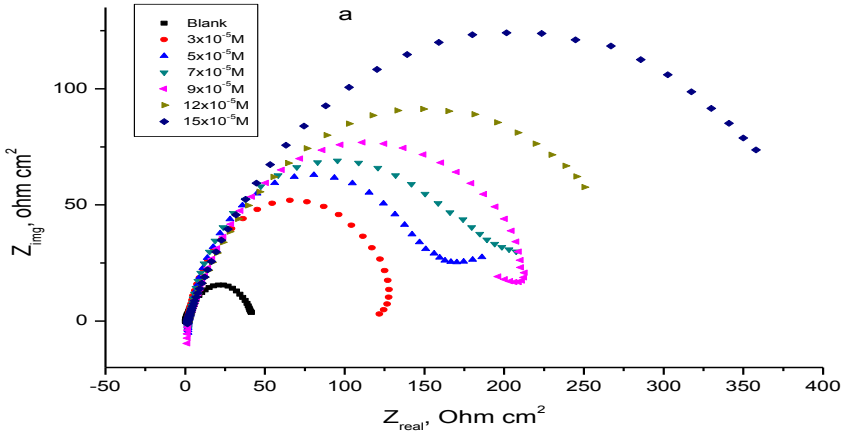

Figure 6a. The Nyquist plots for corrosion of α-brass in 1 M HNO_3in the absence and presence of different concentrations of indole at 25°C

3.6 Electrochemical frequency modulation measurements (EFM)
The EFM is a nondestructive corrosion measurement technique that can directly give values of the corrosion current without prior knowledge of Tafel constants.Like EIS; it is a small ac signal. It is generally accepted that in most cases, the corrosion rates determined with the EFM technique, are much higher than the values determined with other techniques exhibiting low corrosion rates [49].The modulation frequencies that are used in the EFM technique are in the capacitive region of the impedance spectra. However, results of the paper showed good agreement of corrosion rates obtained with the Tafel extrapolation method and are presented in Figs. 8a-8f are examples of α-brass immersed in 1 M HNO_3 solutions in presence of different concentrations of 2-oxyindole.some devoid of investigated compounds and others containing different concentrations of investigated compounds at 25°C. Each spectrum is a current response as a function of frequency.

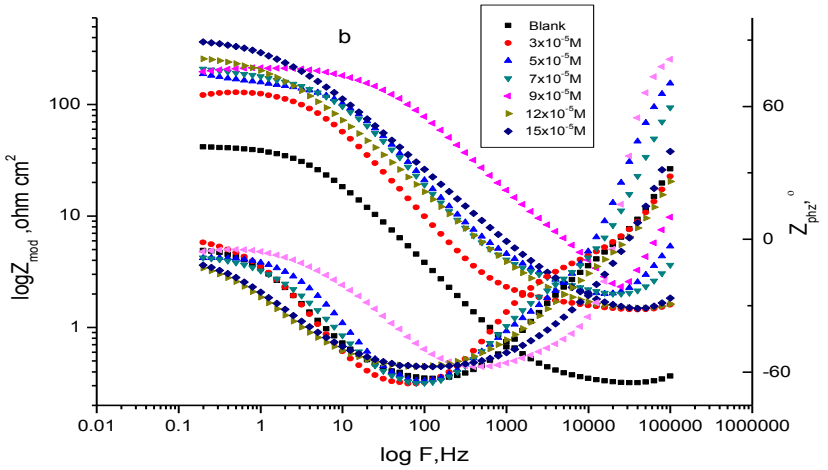

Figure 6b. The Bode plots for corrosion of α-brass in 1 M HNO_3 in the absence and presence of different concentrations of indole at 25°C

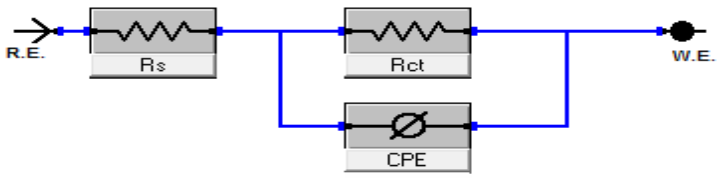

Figure 7. Electrical equivalent circuit model used to fit the results of impedance

Table 5. EIS data of α-brass in 1 M HNO_3 and in the absence and presence of different concentrations of investigated inhibitors at 25 ºC

inhibitors	Concentrations, M	R_{ct}, Ω cm^2	C_{dl}, μF cm^{-2}	Θ	IE%
1 M HNO_3		42.08	754	-------	------
indole	$3x10^{-5}$	129.90	307	0.676	67.6
	$5x10^{-5}$	168.00	255	0.750	75.0
	$7x10^{-5}$	194.30	200	0.783	78.3
	$9x10^{-5}$	207.70	179	0.797	79.7
	$12x10^{-5}$	282.90	139	0.851	85.1
	$15x10^{-5}$	389.40	111	0.892	89.2
2-Oxyindole	$3x10^{-5}$	152.60	312	0.724	72.4
	$5x10^{-5}$	276.30	308	0.848	84.8
	$7x10^{-5}$	351.00	254	0.880	88.0
	$9x10^{-5}$	412.70	119	0.898	89.8
	$12x10^{-5}$	549.30	60	0.923	92.3
	$15x10^{-5}$	854.20	24.1	0.951	95.1

The calculated corrosion kinetic parameters at different concentrations of the investigated compounds 1 M HNO_3at 25 °C (i_{corr}, β_a, β_c, CF-2, CF-3 and % IE) are given in Table 6. From Table 6, the corrosion current densities decrease by increasing the concentration of investigated compounds and the efficiency of inhibition increases by increasing investigated compounds concentrations. The causality factors in Table 6 are very close to theoretical values which according to EFM theory [26, 50] should guarantee the validity of Tafel slopes and corrosion current densities. Values of causality factors in Table 3 indicate that the measured data are of good quality. The standard values for CF-2 and CF-3 are 2.0 and 3.0, respectively. The deviation of causality factors from their ideal values might be due to the perturbation amplitude was too small or that the resolution of the frequency spectrum is not high enough. Another possible explanation is that the inhibitor is not performing very well. The obtained results showed good agreement of corrosion kinetic parameters obtained with the EFM, Tafel extrapolation and EIS methods.

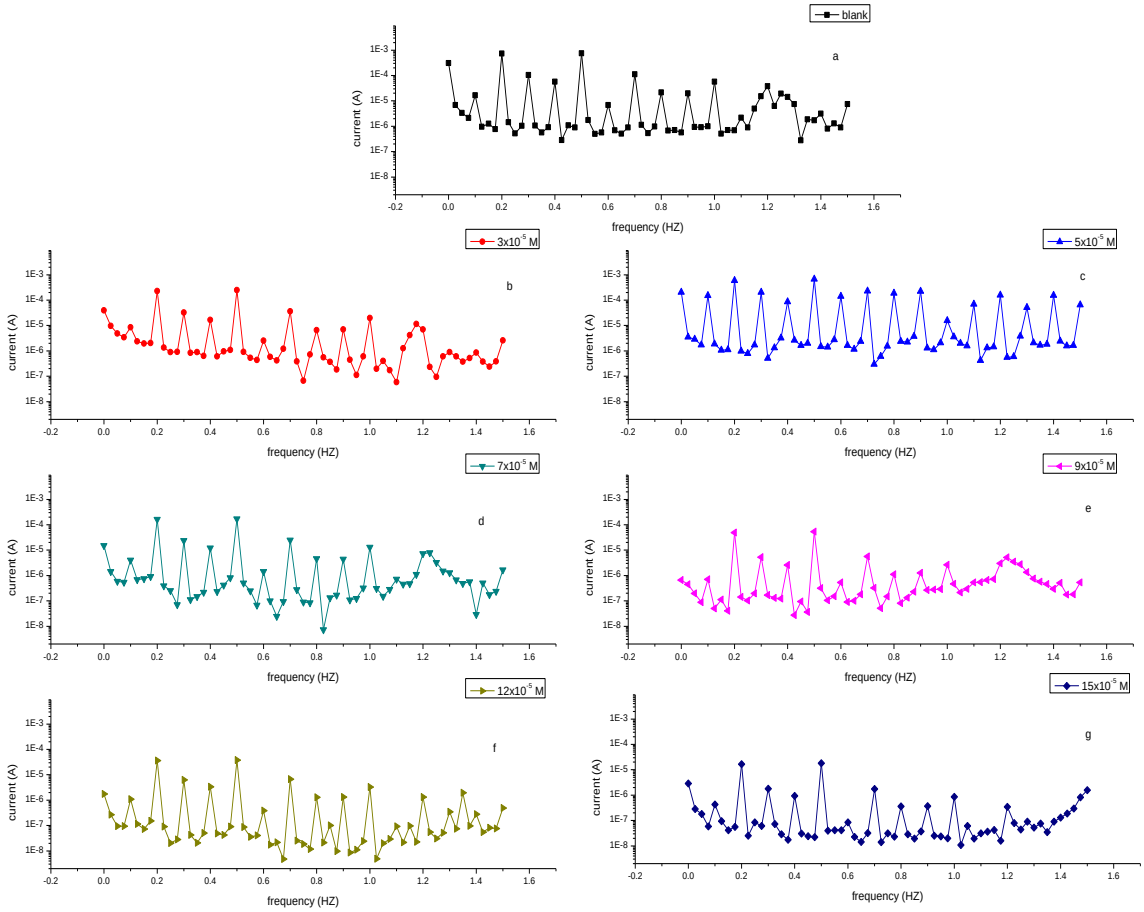

Figures. 8a- 8g. Intermodulation spectrum for α-brass in 1 M HNO_3 solutions without and with various concentrations ($3x10^{-5}$-$15x10^{-5}$M) of 2-oxyindole at 25°C.

The calculated corrosion kinetic parameters at different concentrations of the investigated compounds 1 M HNO_3at 25 °C (i_{corr}, β_a, β_c, CF-2, CF-3 and % IE) are given in Table 6. From Table 6, the corrosion current densities decrease by increasing the concentration of investigated compounds and the efficiency of inhibition increases by increasing investigated compounds concentrations. The causality factors in Table 6 are very close to theoretical values which according to EFM theory [26, 50] should guarantee the validity of Tafel slopes and corrosion current densities. Values of causality factors in Table 3 indicate that the measured data are of good quality. The standard values for CF-2 and CF-3 are 2.0 and 3.0, respectively. The deviation of causality factors from their ideal values might be due to the perturbation amplitude was too small or that the resolution of the frequency spectrum is not high enough. Another possible explanation is that the inhibitor is not performing very well. The obtained results showed good agreement of corrosion kinetic parameters obtained with the EFM, Tafel extrapolation and EIS methods.

3.7 Quantum chemical parameters of investigated compounds

The E_{HOMO} indicates the ability of the molecule to donate electrons to an appropriated acceptor with empty molecular orbitals, whereas the E_{LUMO} indicates its ability to accept electrons. The lower the value of E_{LUMO}, the more ability of the molecule is to accept electrons [51]. The higher the value of E_{HOMO} of the inhibitor, the easier is its ability to offer electrons to the unoccupied d-orbital of metal surface, and the greater is its inhibition efficiency. As is seen from Table 7, there are only small differences (less than 0.08 eV) between the values of E_{HOMO} for the different molecules, which indicate that these molecules have very similar capacities of charge donation to the metallic surface. It was found that the variation of the calculated LUMO energies among all investigated inhibitors is rule less, and the inhibition efficiency is misrelated to the changes of the E_{LUMO}Table 7.
The HOMO–LUMO energy gap, ΔE approach, which is an important stability index, is applied to develop theoretical models for explaining the structure and conformation barriers in many molecular systems. The smaller the value of ΔE, the more is the probable inhibition efficiency the compound has [52-54]. The dipole moment μ,

electric field, was used to discuss and rationalize the structure [55, 56]. It was shown from (Table 7) that 2-oxyindole molecule has the smallest HOMO–LUMO gap compared with the other molecules. Accordingly, it could be expected that 2-oxyindole molecule has more inclination to adsorb on the metal surface than the other molecules.

Table 6. Electrochemical kinetic parameters obtained by EFM technique for α-brass in the absence and presence of different concentrations of investigated compounds in 1 M HNO_3 at 25°C

Inh	Conc., M	i_{corr}, μA cm^{-2}	βa, $mVdec^{-1}$	βc, $mV\ dec^{-1}$	C R, mpy	CF-2	CF-3	θ	IE%
indole	blank	846.4	55.7	111.6	417.7	1.90	3.10		
	$3x10^{-5}$	384.7	55.2	122.4	189.8	1.86	3.34	0.546	54.6
	$5x10^{-5}$	258.7	34.5	37.9	127.7	1.85	2.88	0.694	69.4
	$7x10^{-5}$	217.6	40.8	53.1	107.4	2.01	3.20	0.743	74.3
	$9x10^{-5}$	177.0	24.2	24.8	87.4	1.37	3.19	0.791	79.1
	$12x10^{-5}$	142.1	47.1	100.8	70.1	1.88	3.37	0.832	83.2
	$15x10^{-5}$	101.9	44.8	141.5	50.3	1.88	2.60	0.880	88.0
2-oxyindole	$3x10^{-5}$	280.5	57.3	115.8	138.4	1.88	3.42	0.669	66.9
	$5x10^{-5}$	228.9	18.9	31.2	112.9	2.25	2.82	0.730	73.0
	$7x10^{-5}$	199.5	57.2	117.6	98.5	1.95	2.73	0.764	76.4
	$9x10^{-5}$	57.2	58.5	94.8	28.2	2.10	2.76	0.932	93.2
	$12x10^{-5}$	43.0	54.1	129.9	21.2	1.94	2.93	0.949	94.9
	$15x10^{-5}$	23.0	67.9	118.2	11.3	1.98	2.95	0.973	97.3

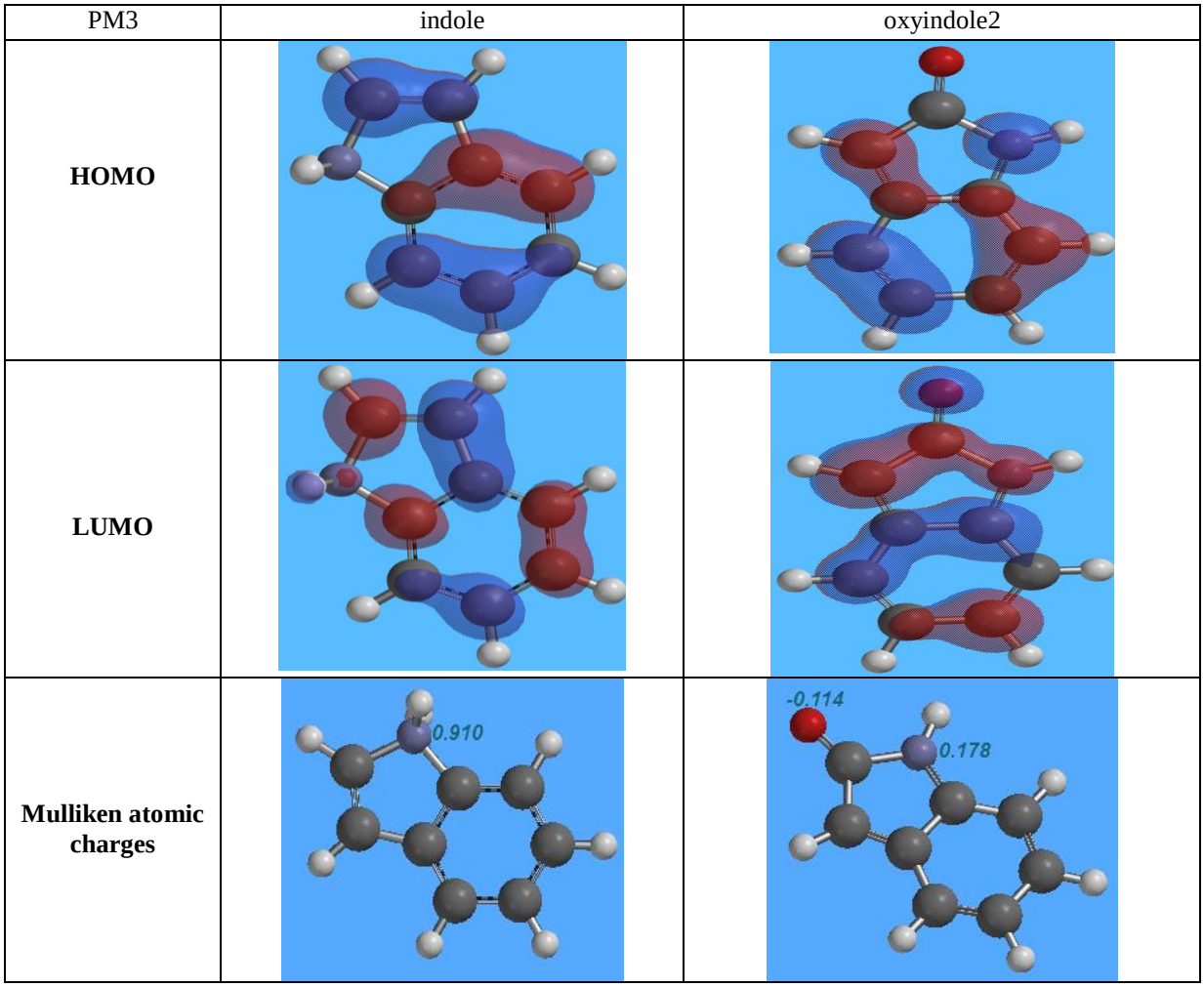

Figure 9. The optimized molecular structures, HOMO, LUMO and Mulliken atomic charges of the inhibitor molecules using PM3

The use of Mulliken population analysis to estimate the adsorption centers of inhibitors has been widely reported and it is mostly used for the calculation of the charge distribution over the whole skeleton of the molecule [57]. There is a general consensus by several authors that the more negatively charged hetero atom is, the more is its ability to adsorb on the metal surface through a donor–acceptor type reaction [58-60]. Variation in the inhibition efficiency of the inhibitors depends on the presence of electronegative O- and N- atoms as substituent in their molecular structure. The calculated Mulliken charges of selected atoms are presented in Fig. 9.

Table7. The calculated quantum chemical parameters for investigated compounds by using PM3

	indole	2-oxyindole
E_{HOMO} (eV)	-13.97	-14.05
E_{LUMO} (eV)	-5.33	-7.30
ΔE (eV)	8.640	6.750
Area ($Å^2$)	151.17	153.97

3.6 Mechanism of Corrosion Inhibition

From the observations drawn from the different methods, corrosion inhibition of α-brass in 1M HNO_3solutions by the investigated inhibitors as indicated from weight loss, potentiodynamic polarization and EIS techniques were found to depend on the concentration and the nature of the inhibitor. The order of inhibition efficiency is as follows: 2-oxyindole > indole

These compounds can beadsorbed in a flat orientation through the nitrogen of the pyrrole ring and oxygen of carbonyl group in case of 2-oxyindole. It wasconcluded that the mode of adsorption depends on the affinityof the metal toward the π-electron clouds of the ring system [61]. Metals, such as Cu and Fe, which have a greateraffinity toward aromatic moieties, were found to adsorb benzene rings in a flat orientation. Thus, it is reasonable to assume that the tested inhibitors are adsorbed in a flat orientation through the N- and O-atoms and π-electrons of the benzene ring. 2-oxyindole has the highest percentage inhibition efficiency. This being due to the presence of an extra carbonylgroup and higher molecular size while indole comes after 2-oxyindole in inhibition efficiency due to the absence of carbonyl group and lower molecular size.

Conclusions

1. Indole and 2-oxyindole have proved to be corrosion inhibitors for corrosion of α-brass in 1M HNO_3 solution
2. The inhibition efficiency increases with increase in the concentration of these inhibitors but decreases with an increase in temperature
3. The inhibition of α-brass alloy in 1 M HNO_3 solution was found to obey Langmuir adsorption isotherm.
4. The thermodynamic values obtained from this study indicate that the presence of the inhibitors increases the activation energy and the negative values of $\Delta G°_{ads}$ indicate spontaneous adsorption of the inhibitors on the surface of α-brass
5. The % IE obtained from electrochemical impedance spectroscopy and potentiodynamic polarization measurements show good agreement with those obtained from weight loss experiments.

References

1. Li S.L., Ma H.Y., Lei S.B.,Yu R., Chen S.H., Liu D.X., *Corrosion* 54 (1998) 947.
2. North, R.F., Pryar M.J., *Corros. Sci*. 10 (1970) 297.
3. Elmorsi, M.A., EL-Sheikh, M.Y., Bastweesy A.M., Ghoneim M.M., *Bull. Electrochem.* 7 (1991) 158.
4. Osman, M.M., *Mater. Chem. Phys*. 71 (2001) 12.
5. Quraishi M.A., Farooqi I.H., Saini P.A., *Br. Corros. J*., 35 (2000) 78.
6. Shih H.C., Tzou R.J., *J. Electrochem. Soc*., 138 (1991) 958.
7. Quartarone G., Moretti G., Bellami T., *Corrosion,* 54 (1998) 606.
8. Gad-Allah A.G., Abou-Romia M.M., Badawy M.W., Rehan H.H., *J. Appl. Electrochem*., 21 (1991) 829.
9. Mitra A.K., *R&D Journal, NTPC* 2 (1996) 52.
10. Elmorsi M.A., Hassanein A.M., *Corros. Sci*., 41 (1999) 2337.
11. Ammeloot F., Fiaud C., Sutter E.M.M., *Electrochim. Acta,* 43 (1997) 3565.
12. Gad Allah A.G., Badawy M.W., Rehan H.H., Abou-Romia M.M., *J. Appl. Electrochem*., 19 (1989) 982.
13. Trabanelli G., Brunoro G., Monticelliand C., Foganolo M., *Corros. Sci*., 25 (1985) 1019.
14. Sylvia da Costa L.F.A., Agostinho M.L., Nobe, K., *J. Electrochem. Soc*., 140 (1993) 3483.
15. Abdallah M., El-Agez M., Fouda A.S., *Int.J.Electrochem.Sci*., 4(2009)336.

16. Fouda A.S., Nazeer A.A., Ashour, E.A., *Zastita Materijala*, 52 (2011) 21.
17. Nazeer A.A., Fouda A.S., Ashour E.A., *J. Mater. Environ. Sci*., 2 (2011)24.
18. Mihit M., Belkhaouda M., Bazzi L., Salghi R., El Issami S., Ait Addi E., *Port. Electrochim. Acta*, 25 (2007) 471.
19. Mihit M., Salghi R.,El Issami, S., Bazzi L., Hammouti B., Ait Addi El., Kertit, S., *Pigment & Resin Technology*, 35 (2006)151.
20. Rehan H. H., Al-Moubarak N. A., Al-Rafai H. A., *Port. Electrochim. Acta*, 21 (2003) 99.
21. Fouda A.S., Mahfouz H., *J. Chil. Chem. Soc*., 54 (2009)302.
22. Fouda A.S., El-Attar K.M., *J. Mater. Eng. Perf.*, 21 (2012) 2352.
23. Mu G.N., Zhao T.P., Liu M., Gu T., *Corrosion*, 52 (1996) 853.
24. Stern M., Geary A. L., *J. Electrochem. Soc*., 104 (1957) 56.
25. Abdel-Rehim S.S., Khaled K.F., Abd-Elshafi N.S., *Electrochim. Acta*, 51 (2006) 3269.
26. Bosch R.W., Hubrecht J., Bogaerts W.F., Syrett B.C., *Corrosion*, 57 (2001) 60.
27. Aljourani J., Raeissi K., Golozar M.A., *Corros. Sci*., 51 (2009) 1836.
28. Dinnappa R. K., Mayanna S. M., *J. Appl. Elcreochem*., 11 (1982) 111.
29. Patel N., Rawat A., Jauhari S., Mehta G., *European J. Chem*., 1 (2010) 129.
30. Langmuir I., *J. Am. Chem. Soc*., 39 (1947) 1848.
31. Bhat J. I., Alva V. D. P., *J. Korean. Chem*. Soc., 55 (2011) 835.
32. Oguzie E. E., Okolue B. N., Ebenso E. E., Onuoha G. M., Onuchukwu A. I., *Mater. Chem. Phys*., 87 (2004) 394.
33. Aramaki K., Hackerman N., *J. Electrochem. Soc*., 116 (1969) 568.
34. Tang L., Li X., Li, L., Mu G., Liu G., *Mater. Chem. Phys*., 97 (2006) 301.
35. Lipkowski J., Ross P.N., Adsorption of Molecules at Metal Electrodes, VCH, New York, (1992)
36. Da Costa S. L. F. A., Agostinho S. M. L., *Corros. Sci*., 45 (1989) 472.
37. El-Sherbiny E.F., *Mater. Chem. Phys*., 60 (1999) 286.
38. Fouda A.S., Al-Sarawy A.A., El-Katori E.E., *Desalination*, 201 (2006) 1.
39. Aljourani J., Raeissi K., Golozar M.A., *Corros. Sci*., 51 (2009)1836.
40. Amar H., Tounsi A., Makayssi A., Derja A., Benzakour J., Outzourhit, A., *Corros. Sci.*, 49 (2007) 2936.
41. Migahed M.A., Azzam E.M.S., Morsy S.M.I., *Corros. Sci*., 51 (2009) 1636.
42. Moussa M.N.H., El-Far A.A., El-Shafei A.A., *Mater. Chem. Phys*., 105 (2007) 105.
43. Benabdellah M.,Touzan R., Aouniti A., Dafali A.S., El-Kadiri S., Hammouti B., Benkaddour M., *Mater. Chem. Phys*., 105 (2007) 373.
44. Bayol E., Kayakirilmaz K., Erbil M., *Mater. Chem.Phys*., 104 (2007) 74.
45. Benalli O., Larabi L., Traisnel M., Gengembra L., Harek Y., *Appl. Surf. Sci.*, 253 (2007) 6130.
46. Hsu C.S., Mansbitfeld F., *Corrosion*, 57 (2001) 747.
47. Epelboin I., Keddam M.,Takenouti H., *J. Appl. Electrochem.*, 2 (1972) 71.
48. Mayer B.J.C., Tuttner K., lorenz W. J., *Electrochim. Acta*, 28 (1983) 171.
49. Kus E., Mansfeld F., *Corros. Sci*., 48 (2006) 965.
50. Gamry Echem Analyst Manual, 2003.
51. Gao G., Liang C., *Electrochim. Acta*, 52 (2007) 4554.
52. Feng Y., Chen S., Guo Q., Zhang Y., Liu G., *J. Electroanal. Chem*., 602 (2007) 115.
53. Gece G., Bilgic S., *Corros. Sci*., 51 (2009) 1876.
54. Martınez S., *Mater. Chem. Phys*., 77 (2002) 97.
55. Ozcan M., Dehri I., Erbil M., *Appl. Surf. Sci*., 236 (2004) 155.
56. Roque J.M., Pandiyan T., Cruz J., Garcia-Ochoa E., *Corros. Sci*., 50 (2008) 614.
57. Kandemirli, F., Sagdinc, S., *Corros. Sci*. 49 (2007) 2118.
58. Bereket G., Ogretic C., Ozsahim C., *J. Mol. Struct., (THEOCHEM)* 663 (2003) 39.
59. Li W., He Q., Pei C., Hou B., *Electrochim. Acta*, 52 (2007) 6386.
60. Rajenran S., *J. Electrochem. Soc.*, 54 (2005) 61.
61. Chauhan L.R., Gunasekaran G., *Corros. Sci.*, 49 (2007) 1143.